CONDENSED MATTER PHYSICS

Breakdown of Hooke's law of elasticity at the Mott critical endpoint in an organic conductor

Elena Gati,[1]* Markus Garst,[2,3] Rudra S. Manna,[1†] Ulrich Tutsch,[1] Bernd Wolf,[1] Lorenz Bartosch,[4] Harald Schubert,[1] Takahiko Sasaki,[5] John A. Schlueter,[6,7] Michael Lang[1]

The Mott metal-insulator transition, a paradigm of strong electron-electron correlations, has been considered as a source of intriguing phenomena. Despite its importance for a wide range of materials, fundamental aspects of the transition, such as its universal properties, are still under debate. We report detailed measurements of relative length changes $\Delta L/L$ as a function of continuously controlled helium-gas pressure P for the organic conductor κ-(BEDT-TTF)$_2$Cu[N(CN)$_2$]Cl across the pressure-induced Mott transition. We observe strongly nonlinear variations of $\Delta L/L$ with pressure around the Mott critical endpoint, highlighting a breakdown of Hooke's law of elasticity. We assign these nonlinear strain-stress relations to an intimate, nonperturbative coupling of the critical electronic system to the lattice degrees of freedom. Our results are fully consistent with mean-field criticality, predicted for electrons in a compressible lattice with finite shear moduli. We argue that the Mott transition for all systems that are amenable to pressure tuning shows the universal properties of an isostructural solid-solid transition.

INTRODUCTION

The Mott metal-insulator transition, driven by strong Coulomb repulsion between electrons (*1*), is a key phenomenon in strongly correlated electron systems. Prime examples for materials where Mott physics is relevant include transition metal oxides (*2*), notably cuprates and manganites, as well as organic charge-transfer salts (*3*, *4*). The strong interest shown to these materials relates to the wealth of intriguing states that was observed to be close to the transition on either side, with spin-liquid phases (*5*, *6*), multiferroicity (*7*, *8*), and unconventional superconductivity (*9*–*11*) being among the most prominent ones. Likewise, the character of the transition itself is of special importance because it is the origin of emergent behavior. The basic notion is that for systems with approximately one electron per lattice site, the electrons become localized once the ratio of Coulomb repulsion U, for two electrons on the same site, over the kinetic energy W exceeds a critical value $(U/W)_c$. Experiments have demonstrated that the Mott transition can be controlled either by doping [as, for example, in the cuprates (*10*)] or by applying pressure P [organic charge-transfer salts (*3*)], giving rise to a first-order transition line. This line terminates in a second-order critical endpoint (Fig. 1A), which is expected to be characterized by universal properties.

The universal properties of the Mott transition continue to be a subject of great interest. For the idealized case of a purely electronic system, as, for example, simulated in cold-atom experiments (*12*), there is strong evidence from theory that the Mott transition shows the universal properties of a liquid-gas transition (*13*, *14*), represented by the Ising universality class, with the double occupancy playing the role of an order parameter. The crucial question is whether this simplified picture can adequately describe the properties of a real material where the critical electronic system is coupled to a compressible lattice. To date, the involvement of the elastic degrees of freedom in the Mott criticality has not been elucidated experimentally. This is remarkable, because the importance of the lattice for the Mott transition can be directly inferred from the fact that the transition can be tuned by pressure, that is, by lattice contraction, which increases the overlap of electronic wave functions on adjacent sites and thereby promotes metallicity. Conversely, the critical electronic system exerts an internal pressure on the elastic system to which the crystal lattice responds. Sufficiently away from the Mott endpoint, the lattice response is weak and acts as a small perturbation on the critical electronic system. However, upon approaching the critical endpoint, the lattice necessarily reacts in a nonperturbative way to the internal strain, implying a vanishing elastic modulus (*15*–*17*), as also shown for the case of piezoelectric ferroelectric criticality (*18*). The fingerprint of this effect would be a strongly nonlinear strain-stress relation, that is, a breakdown of Hooke's law of elasticity. Because of the long-ranged shear forces of the crystal lattice, this breakdown is expected to be accompanied by a crossover to Landau criticality characterized by mean-field critical exponents (Fig. 1A). The remarkable consequence would be that, although the Mott transition is driven by strong electronic correlations, the critical behavior around the endpoint is eventually governed by the universal properties of a solid-solid transition (*17*, *19*) with the strain field becoming a primary order parameter. Measurements of the strain are thus an ideal tool to probe the criticality of the finite-temperature Mott endpoint.

RESULTS

Here, we use measurements of relative length changes for directly probing the lattice effects around the Mott transition. By the combination of capacitive dilatometry with continuously controllable helium-gas pressure (*20*), we can perform high-resolution measurements of relative length changes, $\Delta L/L$, both as a function of temperature at constant pressure and as a function of pressure at constant temperature. The material selected for our study is the quasi–two-dimensional (quasi-2D) organic charge-transfer salt κ-(BEDT-TTF)$_2$Cu[N(CN)$_2$]Cl (abbreviated as κ-Cl hereafter). The reason for choosing this material is twofold. First, this material is situated right on the verge of the Mott

[1]Physikalisches Institut, Goethe-Universität Frankfurt, Max-von-Laue-Straße 1, 60438 Frankfurt am Main, Germany. [2]Institut für Theoretische Physik, Universität zu Köln, Zülpicher Straße 77, 50937 Köln, Germany. [3]Institut für Theoretische Physik, Technische Universität Dresden, Zellescher Weg 17, 01062 Dresden, Germany. [4]Institut für Theoretische Physik, Goethe-Universität Frankfurt, Max-von-Laue-Straße 1, 60438 Frankfurt am Main, Germany. [5]Institute for Materials Research, Tohoku University, Katahira 2-1-1, Sendai 980-8577, Japan. [6]Division of Materials Research, National Science Foundation, Arlington, VA 22230, USA. [7]Materials Science Division, Argonne National Laboratory, Argonne, IL 60439, USA.
*Corresponding author. Email: gati@physik.uni-frankfurt.de (E.G.); michael.lang@physik.uni-frankfurt.de (M.L.)
†Present address: Experimentalphysik VI, Elektronische Korrelationen und Magnetismus, Universität Augsburg, 86159 Augsburg, Germany.

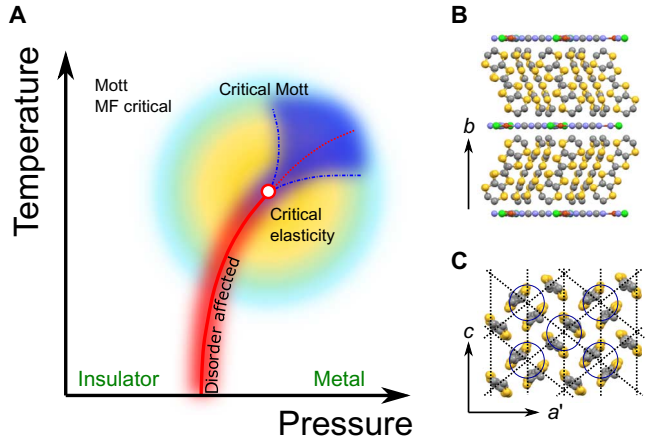

Fig. 1. Generic phase diagram for a pressure-tuned Mott transition and structure of κ-(BEDT-TTF)$_2$Cu[N(CN)$_2$]Cl. (**A**) Generic temperature-pressure phase diagram predicted for the Mott metal-insulator transition in a real material. The red solid line represents the first-order transition line that ends in a second-order critical endpoint (open red circle). The *Widom* line (red dotted line) corresponds to a smooth extrapolation of the first-order line. Blue broken lines (blue-shaded area) represent the predicted crossover lines (crossover regime) that emanate from the critical endpoint (for details, see text). In a distinct region around the critical endpoint, critical elasticity with mean-field (MF) behavior is expected (yellow circle). Further away from the endpoint (light blue circle), within a radius given by the Ginzburg criterion, nontrivial critical exponents of the Mott transition prevail. Outside of this range (white area), the critical properties can be described by a mean-field theory. The pink-shaded area indicates the finite width of the first-order transition due to the presence of some disorder in real systems. (**B**) Structure of κ-(BEDT-TTF)$_2$Cu[N(CN)$_2$]Cl along the out-of-plane *b* axis. For simplicity, the hydrogen atoms are omitted. (**C**) View on the BEDT-TTF plane (*ac* plane). Circles represent one dimer consisting of two BEDT-TTF molecules. The dimers are arranged on a triangular lattice with hopping parameters *t* and *t*′ (dotted lines). *a*′ accounts for a small tilt of the *a* axis with respect to the *b* axis due to the inclination of the BEDT-TTF molecules.

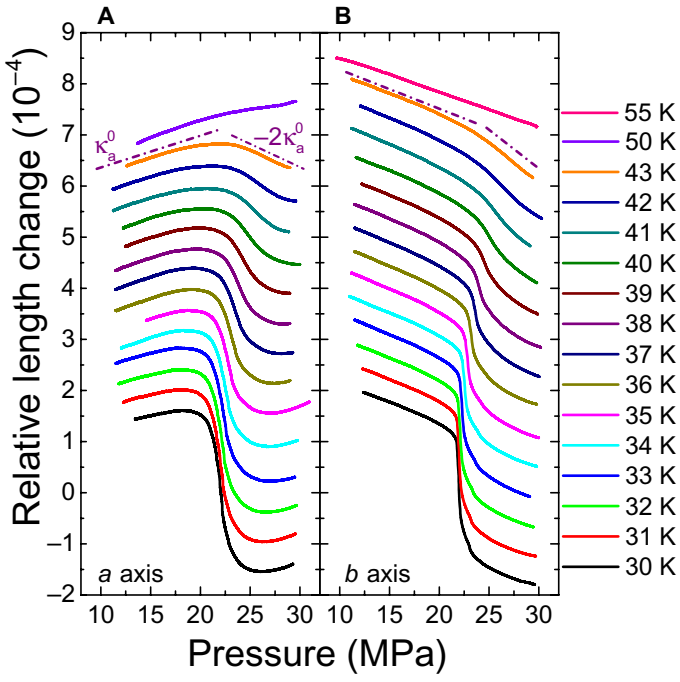

Fig. 2. Relative length changes as a function of pressure. Relative length changes, $\Delta L_i/L_i$, as a function of applied pressure at constant temperatures between 30 and 55 K. Measurements have been performed along the $i = a$ (**A**) and *b* axes (**B**). The data have been offset for clarity. The broken lines close to the data at 43 K, that is, distinctly above $T_c \approx 36.5$ K of the critical endpoint, are guides to the eyes and serve to estimate the pressure-induced changes in the compressibilities. The strong nonlinearities, which are observed here, reflecting nonlinear strain-stress relations, highlight a breakdown of Hooke's law of elasticity.

transition (*21*, *22*) so that moderate pressure $P \lesssim 30$ MPa is sufficient to cover a wide-enough range around the critical endpoint. Second, for this material, a considerably large elasticity-governed critical regime around the critical endpoint has been predicted (*17*). The present study, which focuses on the critical elasticity, goes beyond previous investigations on the critical properties of this and other materials via conductivity (*23*–*25*) and nuclear magnetic resonance (*26*) measurements, where only electronic degrees of freedom have been considered.

The κ-Cl system crystallizes in the orthorhombic *Pnma* structure (*27*) in which the organic BEDT-TTF layers, where BEDT-TTF stands for bis(ethylenedithio)tetrathiafulvalene, alternate with the polymeric anion layers along the *b* axis (Fig. 1B); see section A in the Supplementary Materials for the effect of pressure on the low-temperature structure. This gives rise to a quasi-2D electronic structure with one hole carrier per $(\text{BEDT-TTF})_2^+$-dimer within the *ac* plane (Fig. 1C), establishing a half-filled conduction band. Measurements have been performed on three different single crystals from different sources, yielding essentially the same results.

Relative length changes across the Mott transition

In Fig. 2, we show results of relative length changes $\Delta L_i/L_i$ measured along the in-plane $i = a$ axis (A) and the out-of-plane *b* axis (B) on the same single crystal as a function of pressure *P* at varying temperatures around the Mott transition. These two uniaxial effects represent the dominant contributions of the Mott transition to the volume expansivity, $(\Delta V/V)_{\text{Mott}} \approx (\Delta L_a/L_a)_{\text{Mott}} + (\Delta L_b/L_b)_{\text{Mott}}$, because there is practically no effect visible along the *c* axis, $(\Delta L_c/L_c)_{\text{Mott}} \approx 0$ (see fig. S1). The data in Fig. 2 disclose two essential aspects. The first aspect concerns the character of the transition and how this character changes with increasing temperature.

For the lowest temperature studied at 30 K, which is well below the critical temperature $T_c \approx 36.5$ K (see below for the determination of T_c), we observe an abrupt, slightly broadened jump of the sample length as a function of pressure along both axes, reflecting the first-order character of the Mott transition. The data reveal a distinct decrease of the *a* and *b* axes lattice parameters while tuning the system from the low-pressure insulating side of the transition to the high-pressure metallic side. This observation is consistent with the notion that the itinerant electrons on the metallic side provide an additional contribution to the cohesion of the solid and supports the notion that $(\Delta V/V)_{\text{Mott}}$ is proportional to the order parameter of the transition. For pressures distinctly below and above the jump, the sample length is changing in an approximately linear manner with pressure, reflecting normal elastic behavior following Hooke's law of elasticity. This elastic background exhibits the usual negative slope for the *b* axis lattice parameter, that is, a shrinking of the lattice with increasing pressure, whereas it shows an unusual positive slope for the *a* axis lattice parameter. We assign this behavior to the Poisson effect as a result of a pressure-induced progressive inclination of the BEDT-TTF molecules with respect to the *b* axis (Fig. 1B). Upon increasing the temperature, the discontinuity gradually decreases and evolves into a continuous crossover behavior at higher temperatures.

The second important aspect contained in Fig. 2 (A and B) relates to the slopes of the $\Delta L_i(P)/L_i$ curves near the critical endpoint, reflecting the material's uniaxial compressibilities $\kappa_i = -d(\Delta L_i/L_i)/dP$ along the $i = a$ and b axes. For temperatures around $T_c \approx 36.5$ K up to at least 43 K, we observe highly nonlinear variations of $\Delta L_i/L_i$ with pressure for both axes over a wide pressure range. This is distinctly different from the usual elastic background behavior characterized by a smooth linear variation with pressure, in leading order. This approximate linear $\Delta L/L$ versus P behavior is revealed for the data set taken at 55 K (for the b axis, Fig. 2B), that is, way above T_c. As exemplarily indicated for the data at 43 K, which is about 6.5 K above T_c, strong variations in $\Delta L_i(P)/L_i$ with pressure, giving rise to two approximately linear regimes with distinctly different slopes, can be identified (broken lines in Fig. 2, A and B). The pressure-induced changes of the compressibilities revealed here are of the order of the compressibilities themselves, that is, $|\Delta\kappa_a^0|/\kappa_a^0 \approx 3$ and $|\Delta\kappa_b^0|/\kappa_b^0 \approx 1$. We assign these drastic effects around (T_c, P_c) to a critical elasticity as a result of the coupling of the critical electronic system to the lattice. The strongly nonlinear strain-stress relation observed here, representing the major result of our study, highlights a breakdown of Hooke's law of elasticity over a considerably wide temperature-pressure range around the Mott transition. We note that indications for strong changes of the compressibility were also seen in previous ultrasonic investigations on the same compound (*28*).

Phase diagram of κ-(BEDT-TTF)$_2$Cu[N(CN)$_2$]Cl

To classify the observed critical behavior and to compare it with theoretical predictions, precise knowledge about the system's phase diagram (Fig. 3), including the location of the Mott transition line, the critical endpoint (T_c, P_c), and the various crossover lines is important. The inflection points of the $\Delta L_i(P)/L_i$ data in Fig. 2 (A and B) define a characteristic line, $P_c(T)$ (Fig. 3), which is separated at the critical endpoint $P_c = P_c(T_c)$ into a first-order transition line for $T < T_c \approx 36.5$ K and the *Widom* line for $T > T_c$. We find a very good agreement of the Mott transition line obtained from our thermodynamic measurements with that of transport experiments (*23*) (see fig. S2). Our preliminary results on the effects of disorder, intentionally introduced into a crystal by x-ray irradiation (*29*), indicate a shift of the Mott transition line to lower pressures (see fig. S3), consistent with results from dynamic mean-field theory (*30*). We consider the good agreement of the phase transition lines, shown in fig. S2, as an indication that the crystals studied here are of similar high quality as those studied by Kagawa *et al.* (*23*). To determine T_c for the present crystal, we have taken two complementary approaches. First, we use the intersection point of the first-order transition line with a crossover line (Fig. 1A), which emanates from the critical point. As previously pointed out (*31*), the maximum response α_{max} in the coefficient of thermal expansion $\alpha(T) = L^{-1}dL/dT$ obtained from temperature-dependent measurements (see fig. S1) provides this crossover feature. Because of the finite slope of the first-order transition line at T_c, these measurements at varying P = const. also allow us to discriminate rounded crossover anomalies, expected for $P > P_c$, from jump-like features, characterizing the state at $P < P_c$. By including the positions of $\alpha_{max}(T, P = \text{const.})$ into the phase diagram and applying the abovementioned criterion, we obtain a critical point at $T_c = (36.5 \pm 0.5)$ K and $P_c = (23.4 \pm 0.2)$ MPa.

A second approach for determining the critical point is provided by considering the width of the various features observed. This criterion also delivers insight into an additional scale that is introduced into the problem by the effects of disorder, relevant for any real material. Even far below the critical endpoint, we observe that the jump in $\Delta L_i/L_i$ is not infinitely sharp but broadened, giving rise to a finite width of the peak in κ_i at P_c that is practically temperature-independent. We assign this broadening to disorder, that is, spatial variations of internal stress induced by impurities and/or other crystal defects. However, upon increasing the temperature sufficiently above the endpoint, the width of the peak in κ_i becomes distinctly larger and strongly temperature-dependent and thus can be attributed to criticality. We estimate the width of the features in $\Delta L_i(P)/L_i$ by the full width at half maximum of the peak in the κ_i data (see fig. S4) and include this information [range delimited by red broken lines for $T < T_c$ and blue broken lines for $T > T_c$ in the phase diagram (Fig. 3)]. A linear extrapolation of these lines from high temperatures above 38 K, where the broadening is governed by criticality so that disorder effects are expected to play a minor role, to lower temperatures yields an intersection point of (36.7 ± 0.5) K, consistent with the abovementioned alternative estimate for T_c.

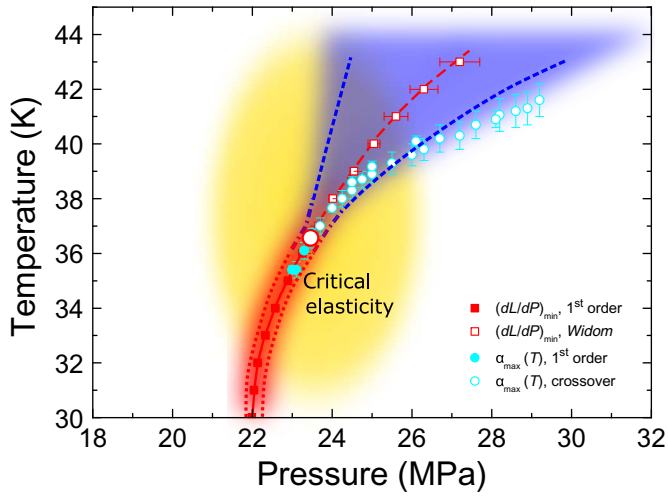

Fig. 3. Experimentally determined temperature-pressure phase diagram for κ-(BEDT-TTF)$_2$Cu[N(CN)$_2$]Cl. Full (open) red squares represent the first-order transition line (*Widom* line). The open red circle indicates the critical endpoint. Full (open) cyan points show the position of maximum response, α_{max}, of the coefficient of thermal expansion, $\alpha(T) = L^{-1}dL/dT$, which can be assigned to a first-order transition line (crossover line). Red- and blue-shaded areas delimited by the broken lines in the same color code indicate the experimentally determined width of the features along the b axis and can be assigned to the disorder-related (red) and the criticality-related (blue) crossover regimes, respectively. The broken lines represent, within the error margins, the full width at half maximum of the peaks in κ_i. The yellow ellipse indicates the range where critical elasticity, characterized by mean-field critical exponents, dominates.

Modeling of the relative length changes

After having pinpointed the critical endpoint (T_c, P_c) to a good degree of accuracy, we can proceed by further analyzing the critical behavior. Note that the disorder broadening of the critical signatures, implying an additional length scale, precludes a conventional one-parameter scaling collapse of the data (see section F, Supplementary Materials). Instead, we quantitatively compare our data to the theoretically expected behavior for a critical electronic system coupled to elastic degrees of freedom, yielding the universal properties of an isostructural solid-solid endpoint (*17*). For an orthorhombic crystal, the elastic constant tensor $C_{\rho\nu}$ in Voigt notation has six nondegenerate eigenvalues whose eigenvectors correspond to three shear and three compressive strain-singlet modes (*32*). One of the latter strain singlets, ε, can be identified with the order parameter of the solid-solid transition, which is

measured by $\Delta L/L$. This strain singlet exactly obeys a mean-field equation that, after appropriate rescaling, reads within Landau theory $r\,\varepsilon + u\,\varepsilon^3 = -\sigma$ (see section F and fig. S5, Supplementary Materials). Close to the endpoint, the dimensionless stress σ is given in terms of the hydrostatic pressure P by $\sigma = -(P - P_c(T))/P_c(T_c)$ with the experimentally determined line $P_c(T)$ and the rigidity $r = (T - T_c)/T_c$, which is proportional to the associated eigenvalue of $C_{\rho\nu}$. We neglect here a possible pressure dependence of the tuning parameter r, which would result in an additional but subleading nonlinearity in the strain-stress relation. Having experimentally determined the line $P_c(T)$ as well as the critical temperature T_c, the mean-field equation is characterized by a single parameter, u, that quantifies the strength of the nonlinear cubic term ε^3. At T_c, the rigidity vanishes ($r = 0$), and the strain singlet responds in a nonlinear fashion to an applied stress, $\varepsilon \sim (-\sigma)^{1/\delta}$, with the mean-field critical exponent $\delta = 3$, signaling the breakdown of Hooke's law.

To account for the disorder broadening in a phenomenological manner, we assume a multidomain state, caused by extrinsic defects of the crystal structure, where, for simplicity, each domain independently contributes to the mean strain. We average the mean-field solution $\varepsilon(r, \sigma, u)$ with a Gaussian stress distribution $P_w(s)$ with a constant variance, w, and zero mean, $\langle \varepsilon(r, \sigma, u)\rangle_w = \int ds P_w(s)\, \varepsilon(r, \sigma + s, u)$, that accounts for long-range stress fluctuations so that $\langle \varepsilon(r, \sigma = 0, u)\rangle_w = 0$. Close to the transition, slight variations of the stress can lead to the simultaneous compression and expansion of different parts of the crystal with the concomitant generation of dislocation defects and grain boundaries. This intrinsically generated disorder, in turn, may influence the stress distribution within the crystal (*33*, *34*), but a full self-consistent treatment of these effects is beyond the scope of the present paper. After normalizing the various data sets in Fig. 2 to their inflection point $P_c(T)$ to eliminate offset contributions due to the temperature-dependent background expansion, the length changes are described by

$$\Delta L_i/L_i = -\kappa_i^0 \left(P - P_c(T)\right) - A_i \left\langle \varepsilon\left((T - T_c)/T_c, -\left(P - P_c(T)\right)/P_c(T_c), u\right)\right\rangle_w \quad (1)$$

Here, κ_i^0 is the background compressibility, and A_i is the proportionality constant between the singlet ε and the relative length change along the direction $i = a, b$. We determine the variance w from a Gaussian fit to the $-d(\Delta L_i/L_i)/dP$ data at 30 K (see fig. S4 and section F, Supplementary Materials), that is, well below the critical point, which yields for the a axis $w_a = 1.3 \times 10^{-3}$ and the b axis $w_b = 4.6 \times 10^{-5}$. Note that $w^{1/2}$ measures the width of the broadening-affected pressure range. The fact that $w_a^{1/2} \approx 5 \times w_b^{1/2}$, as is already apparent from the bare data in Fig. 2, indicates that more, slightly different domain states contribute to the relative length change along the a axis than along the b axis. This implies strongly anisotropic domains, being elongated perpendicular to the planes, which can be rationalized by considering the spatial anisotropy inherent to the structure of κ-Cl (see fig. S6). As demonstrated in Fig. 4, fits based on Eq. 1 with only three parameters—u, κ_i^0, and A_i for $i = b$—provide an excellent description of the whole data set along the b axis covering a pressure range of 15 MPa $\lesssim P \lesssim$ 30 MPa at 14 different temperatures of 30 K $\leq T \leq$ 43 K (see fig. S7 for corresponding fits to the a axis data). For the dimensionless parameter u quantifying the nonlinearity of the Landau potential, we find $u = 0.18$. For the noncritical contribution, we obtain $\kappa_b^0 = 4 \times 10^{-6}$ MPa^{-1}, which is of the same order as the background compressibility reported for a related material (*35*). The individual fits to the various T = const. data sets yield slightly different values for the proportionality constant A_b, which, however, follow to a good approximation a T linear variation $A_b = (0.86 - 1.01\,(T - T_c)/T_c) \times 10^{-4}$ (see fig. S8). We assign this effect to a smooth T dependence of the elastic tensor $C_{\rho\nu}$ affecting its eigenvalues and eigenvectors. We stress that a description of equally high quality is also obtained for the a axis data with identical u but different $\kappa_a^0 \neq \kappa_b^0$ and $A_a \neq A_b$ (see fig. S7). Note that by changing the critical temperature within the indicated error margin, fits of equal quality are obtained with A_i values changing by 5% at maximum. Likewise, treating the critical temperature as an additional free parameter in the fitting procedure yields $T_c = 36.2$ K, consistent with the independently determined value of $T_c = (36.5 \pm 0.5)$ K. Taken together, the pronounced and strongly nonlinear lattice effects observed along the a and b axes of κ-Cl around its Mott transition can be well described on a quantitative level by mean-field criticality, as

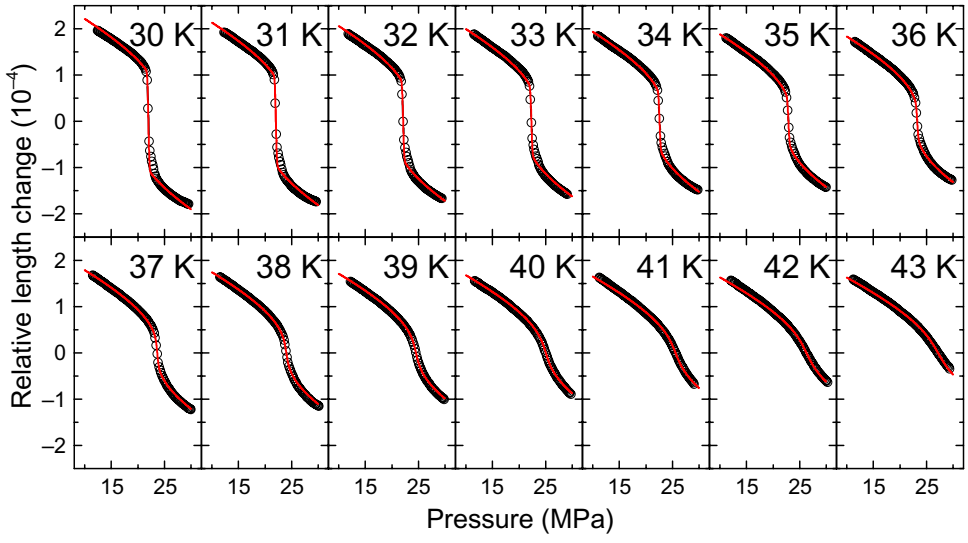

Fig. 4. Modeling of relative length changes. Measurements of the relative length change $\Delta L_b(P)/L_b$ at various constant temperatures around $T_c \approx 36.5$ K as a function of pressure (black symbols) along the b axis, together with a fit of the mean-field solution based on Eq. 1 (red solid line; for details, see text).

expected for a critical electronic system coupled to lattice degrees of freedom. We stress that mean-field criticality is also revealed in an independent approach based on the analysis of power-law dependencies in $\Delta L_b/L_b$ with respect to temperature and pressure upon approaching the critical endpoint (see section I, figs. S9 to S11, and table S1, Supplementary Materials).

DISCUSSION

The raw data (Fig. 2) together with the fits based on Eq. 1 (Fig. 4) allow for a classification of the different scales involved. We find critically renormalized compressibilities κ_i around (T_c, P_c) = (36.5 K, 23.4 MPa) extending up to at least 43 K in temperature and up to about 25 MPa in pressure. This corresponds to a T-P range of critical elasticity of width $\Delta T/T_c \approx 20\%$ and $\Delta P/P_c \approx 10\%$ (yellow-shaded regime in Fig. 3). From this finding, we conclude that critical elasticity prevails in κ-Cl and that mean-field criticality governs its Mott endpoint. Note that critical elasticity can also be concluded (*36*) for the archetype Mott system V_2O_3, which is situated somewhat off the transition on the metallic side, where a substantial softening of one of the elastic constants has been observed (*37*).

At larger distances from the endpoint, where the lattice response becomes weak and acts as a small perturbation, a crossover to electronic criticality is expected with mean-field or nontrivial Ising exponents depending on the size of the underlying Ginzburg regime (blue-shaded regime in Fig. 1A). Whether this Ginzburg range exceeds the critical elastic regime (yellow-shaded regime in Fig. 1A) in the present system cannot be answered on the basis of the available data. However, the fact that thermal expansion measurements on a related system (*31*), the chemical pressure of which corresponds to $(P - P_c)/P_c \approx 20\%$, were found to be consistent with 2D Ising criticality may indicate that the Ginzburg regime actually exceeds the mean-field regime for this material class. Moreover, we find that the width of the critical elasticity regime in pressure is a factor of 10 larger in comparison to the disorder-affected broadening regime, indicating that in this clean sample, disorder is only a minor effect and can be effectively treated within the framework of critical elasticity.

The critical elasticity revealed here for κ-Cl highlights the significance of strain measurements in probing the criticality of a finite-temperature Mott endpoint. At the same time, our result demonstrates that more theoretical work is needed to include the aspect of critical elasticity in the analysis of conductivity data (*23*), the relation of which to the order parameter is intricate (*38*) and whose classical critical signatures develop on a strongly varying background that has been assigned to quantum criticality (*39*, *40*).

Because of the long-range nature of the shear forces, mean-field criticality of an isostructural critical endpoint implies the absence of a diverging correlation length (*32*, *36*). As a consequence, one would expect that the critical slowing down observed by Hartmann *et al.* (*41*) saturates sufficiently close to the endpoint, provided that it is associated with a phonon mode. Alternatively, it could also arise from the slow dynamics associated with domain formation due to disorder. Further studies are required to identify the origin of the slowing down in κ-Cl close to its Mott endpoint.

In summary, our results presented for the organic conductor κ-(BEDT-TTF)$_2$Cu[N(CN)$_2$]Cl highlight the relevance of lattice degrees of freedom in the description of universal properties of the Mott transition in real materials, that is, in the presence of a compressible lattice. Whenever the Mott transition can be tuned by pressure, which is the case for many systems, such as various κ-(BEDT-TTF)$_2X$ (*21*, *22*, *42*) or Et$_x$Me$_{4-x}Z$[Pd(dmit)$_2$]$_2$ (*43*) organic charge-transfer salts, as well as transition metal oxides, such as $(V_{1-x}M_x)_2O_3$ (*24*, *44*–*46*), NiO (*47*), or $PbCrO_3$ (*48*), the Mott endpoint will eventually be governed by critical elasticity. A different situation is encountered in VO_2, where doping experiments suggest that the transition is insensitive to pressure so that the elastic coupling is expected to be weak. For this system, an extended regime was observed where the Mott criticality is governed by the random-field Ising model (*49*). Generally, the steeper the first-order transition line is in the T-P phase diagram, the larger the size of the critical elastic regime should be. According to the Clausius-Clapeyron equation, the slope of this line dT_c/dP is given by $\Delta V/\Delta S$, that is, the ratio of the volume change to the change of entropy across the first-order transition. Because ΔS has to vanish for $T_c \rightarrow 0$, implying an increase of dT_c/dP, the range of critical elasticity is expected to grow for materials with lower critical temperature. However, irrespective of the width of this regime, our results demonstrate that the Mott transition in a real material with a finite shear modulus sufficiently close to the endpoint shows the universal properties of an isostructural solid-solid endpoint with mean-field critical exponents rather than a liquid-gas endpoint.

MATERIALS AND METHODS

Measurements of the relative length changes were performed by using a capacitive dilatometer (*50*, *51*), enabling length changes of $\Delta L \geq 5 \times 10^{-3}$ nm to be resolved. By combining the dilatometer with a continuously controllable helium-gas pressure system, in which the pressure cell is connected by a capillary to a room-temperature pressure reservoir, we could perform measurements both as a function of temperature at constant pressure and as a function of pressure at constant temperature (*20*). In this capacitive technique, length changes were calculated from the measured changes of the capacitance of a plate capacitor; see the work by Pott and Schefzyk (*51*) for technical details. To account for effects that are related to temperature-dependent and pressure-dependent changes of the dielectric function ϵ_r of the pressure-transmitting medium helium, a quantity that is relevant for the data processing, $\epsilon_r(T, P)$ was determined from independent measurements on a standard material (aluminum) at the same temperatures where T = const. measurements on κ-Cl were performed. During a pressure sweep, the temperature is stabilized within ± 0.1 mK on short term (30 min) and $|\Delta T| < 15$ mK on long term (24 hours). The pressure changes, with a typical rate of 1.5 MPa/hour, could be determined with a resolution of $|\Delta P| \leq 0.03$ MPa. For technical reasons, pressure sweeps could only be performed under decreasing pressure, precluding the measurements of hysteresis loops. During temperature sweeps, which had been performed upon warming at a slow rate of 1.5 K/hour, the pressure was kept constant within $|\Delta P| \leq 0.05$ MPa. To hold the crystal in the dilatometer cell, a small uniaxial force (typically 0.2 to 0.8 N) has to be applied to the crystal. The corresponding uniaxial pressure depends on the cross-sectional area of the crystal studied. For the measurements along the a and b axes shown in Fig. 2 (A and B), the uniaxial pressure components were estimated to 0.4 and 0.8 MPa, respectively (see fig. S12 and section J, Supplementary Materials).

In total, three different crystals from different sources were studied and found to show similar behavior. For crystal #063-1, as discussed here in the main text, data were taken along all three axes. The results were cross-checked by measurements along the a axis for crystals #063-2 and #5-1. These crystals, with typical dimensions $a \times b \times c \approx 0.7 \times 1 \times 0.5$ mm^3 were grown following the standard electrochemical procedure

(*52*). Before the measurements, the crystals were cooled through the glass transition $T_g \approx 67$ K by using a slow cooling rate of −3 K/hour to reduce disorder in the ethylene end groups of the BEDT-TTF molecules (*53*).

SUPPLEMENTARY MATERIALS

Supplementary material for this article is available at http://advances.sciencemag.org/cgi/content/full/2/12/e1601646/DC1

section A. Structure information for κ-$(BEDT\text{-}TTF)_2Cu[N(CN)_2]Cl$

section B. Measurements of relative length changes performed as a function of temperature at constant pressure

section C. Phase transition and *Widom* line from thermodynamic versus conductivity measurements

section D. Effects of x-ray irradiation on the first-order Mott transition

section E. Measurements of relative length changes performed as a function of pressure at constant temperature

section F. Theory of critical elasticity for the solid-solid endpoint in κ-Cl

section G. Disorder affected broadening of the signatures below T_c

section H. Quantitative modeling of relative length changes along the *a* axis as a function of pressure around the critical endpoint

section I. Independent estimate of critical exponents

section J. Effect of a small uniaxial pressure exerted by the dilatometer cell

fig. S1. Uniaxial coefficients of thermal expansion.

fig. S2. Phase transition and *Widom* line from thermodynamic versus conductivity measurements.

fig. S3. Effects of x-ray irradiation on the first-order Mott transition.

fig. S4. Uniaxial compressibilities.

fig. S5. Effect of higher-order couplings.

fig. S6. Schematic representation of the domain formation in κ-Cl.

fig. S7. Modeling of the relative length changes along the *a* axis.

fig. S8. Variation of the fit parameter A_i as a function of temperature.

fig. S9. Scheme of the scans in the phase diagram unraveling the different critical exponents.

fig. S10. Estimate of critical exponent δ.

fig. S11. Estimate of critical exponents β and γ.

fig. S12. Effect of a small uniaxial pressure exerted by the dilatometer cell.

table S1. Set of critical exponents β, γ, and δ of various universality classes.

References (*54*–*57*)

REFERENCES AND NOTES

1. N. F. Mott, *Metal-Insulator Transition* (WILEY-VCH Verlag, 1990).
2. M. Imada, A. Fujimori, Y. Tokura, Metal-insulator transitions. *Rev. Mod. Phys.* **70**, 1039–1263 (1998).
3. K. Kanoda, Recent progress in NMR studies on organic conductors. *Hyperfine Interact.* **104**, 235–249 (1997).
4. N. Toyota, M. Lang, J. Müller, *Low-Dimensional Molecular Metals* (Springer-Verlag, Berlin Heidelberg, 2007).
5. Y. Shimizu, K. Miyagawa, K. Kanoda, M. Maesato, G. Saito, Spin liquid state in an organic Mott insulator with a triangular lattice. *Phys. Rev. Lett.* **91**, 107001 (2003).
6. L. Balents, Spin liquids in frustrated magnets. *Nature* **464**, 199–208 (2010).
7. T. Kimura, T. Goto, H. Shintani, K. Ishizaka, T. Arima, Y. Tokura, Magnetic control of ferroelectric polarization. *Nature* **426**, 55–58 (2003).
8. P. Lunkenheimer, J. Müller, S. Krohns, F. Schrettle, A. Loidl, B. Hartmann, R. Rommel, M. de Souza, C. Hotta, J. A. Schlueter, M. Lang, Multiferroicity in an organic charge-transfer salt that is suggestive of electric-dipole-driven magnetism. *Nat. Mater.* **11**, 755–758 (2012).
9. M.-S. Nam, A. Ardavan, S. J. Blundell, J. A. Schlueter, Fluctuating superconductivity in organic molecular metals close to the Mott transition. *Nature* **449**, 584–587 (2007).
10. P. A. Lee, N. Nagaosa, X.-G. Wen, Doping a Mott insulator: Physics of high-temperature superconductivity. *Rev. Mod. Phys.* **78**, 17–85 (2006).
11. B. Keimer, S. A. Kivelson, M. R. Norman, S. Uchida, J. Zaanen, From quantum matter to high-temperature superconductivity in copper oxides. *Nature* **518**, 179–186 (2015).
12. M. Greiner, O. Mandel, T. Esslinger, T. W. Hänsch, I. Bloch, Quantum phase transition from a superfluid to a Mott insulator in a gas of ultracold atoms. *Nature* **415**, 39–44 (2002).
13. C. Castellani, C. Di Castro, D. Feinberg, J. Ranninger, New model Hamiltonian for the metal-insulator transition. *Phys. Rev. Lett.* **43**, 1957–1960 (1979).
14. G. Kotliar, E. Lange, M. J. Rozenberg, Landau theory of the finite temperature Mott transition, *Phys. Rev. Lett.* **84**, 5180–5183 (2000).
15. P. Majumdar, H. R. Krishnamurthy, Lattice contraction driven insulator-metal transition in the $d = \infty$ local approximation. *Phys. Rev. Lett.* **73**, 1525–1528 (1994).
16. S. R. Hassan, A. Georges, H. R. Krishnamurthy, Sound velocity anomaly at the Mott transition: Application to organic conductors and V_2O_3. *Phys. Rev. Lett.* **94**, 036402 (2005).
17. M. Zacharias, L. Bartosch, M. Garst, Mott metal-insulator transition on compressible lattices. *Phys. Rev. Lett.* **109**, 176401 (2012).
18. A. P. Levanyuk, A. A. Sobyanin, Second-order phase transitions without divergences in the second order derivatives of the thermodynamic potential. *Zh. Eksp. Teor. Fiz. Pis. Red.* **11**, 540–543 (1970).
19. T. Chou, D. R. Nelson, Dislocation-mediated melting near isostructural critical points. *Phys. Rev. E Stat. Phys. Plasmas Fluids Relat. Interdiscip. Topics* **53**, 2560–2570 (1996).
20. R. S. Manna, B. Wolf, M. de Souza, M. Lang, High-resolution thermal expansion measurements under helium-gas pressure. *Rev. Sci. Instrum.* **83**, 085111 (2012).
21. S. Lefebvre, P. Wzietek, S. Brown, C. Bourbonnais, D. Jérome, C. Mézière, M. Fourmigué, P. Batail, Mott transition, antiferromagnetism, and unconventional superconductivity in layered organic superconductors. *Phys. Rev. Lett.* **85**, 5420–5423 (2000).
22. P. Limelette, P. Wzietek, S. Florens, A. Georges, T. A. Costi, C. Pasquier, D. Jérome, C. Mézière, P. Batail, Mott transition and transport crossovers in the organic compound κ-$(BEDT\text{-}TTF)Cu[N(CN)_2]Cl$. *Phys. Rev. Lett.* **91**, 016401 (2003).
23. F. Kagawa, K. Miyagawa, K. Kanoda, Unconventional critical behaviour in a quasi-two-dimensional organic conductor. *Nature* **436**, 534–537 (2005).
24. P. Limelette, A. Georges, D. Jérome, P. Wzietek, P. Metcalf, J. M. Honig, Universality and critical behavior at the Mott transition. *Science* **302**, 89–92 (2003).
25. M. Abdel-Jawad, R. Kato, I. Watanabe, N. Tajima, Y. Ishii, Universality class of the Mott transition. *Phys. Rev. Lett.* **114**, 106401 (2015).
26. F. Kagawa, K. Miyagawa, K. Kanoda, Magnetic Mott criticality in a κ-type organic salt probed by NMR. *Nat. Phys.* **5**, 880–884 (2009).
27. J. M. Williams, A. M. Kini, H. H. Wang, K. D. Carlson, U. Geiser, L. K. Montgomery, G. J. Pyrka, D. M. Watkins, J. M. Kommers, From semiconductor–semiconductor transition (42 K) to the highest-T_c organic superconductor, κ-$(ET)_2Cu[N(CN)_2]Cl$ (T_c = 12.5 K). *Inorg. Chem.* **29**, 3272–3274 (1990).
28. D. Fournier, M. Poirier, M. Castonguay, K. D. Truong, Mott transition, compressibility divergence, and the *P-T* phase diagram of layered organic superconductors: An ultrasonic investigation. *Phys. Rev. Lett.* **90**, 127002 (2003).
29. T. Sasaki, Mott-Anderson transition in molecular conductors: Influence of randomness on strongly correlated electrons in the κ-$(BEDT\text{-}TTF)_2X$ system. *Crystals* **2**, 374–392 (2012).
30. K. Byczuk, W. Hofstetter, D. Vollhardt, Mott-Hubbard transition versus Anderson localization in correlated electron systems with disorder. *Phys. Rev. Lett.* **94**, 056404 (2005).
31. L. Bartosch, M. de Souza, M. Lang, Scaling theory of the Mott transition and breakdown of the Grüneisen scaling near a finite-temperature critical end point. *Phys. Rev. Lett.* **104**, 245701 (2010).
32. R. A. Cowley, Acoustic phonon instabilities and structural phase transitions. *Phys. Rev. B* **13**, 4877–4885 (1976).
33. T. Nattermann, Instabilities in Ising systems with short- and long-range-correlated quenched random fields. *J. Phys. C Solid State* **16**, 6407–6413 (1983).
34. J. Burgy, A. Moreo, E. Dagotto, Relevance of cooperative lattice effects and stress fields in phase-separation theories for CMR manganites. *Phys. Rev. Lett.* **92**, 097202 (2004).
35. D. Chasseau, J. Gaultier, M. Rahal, L. Ducasse, M. Kurmoo, P. Day, Pressure dependence of the structural and electronic properties of the molecular superconductor, κ-$(BEDT\text{-}TTF)_2Cu(NCS)_2$. *Synth. Met.* **42**, 2039–2042 (1991).
36. M. Zacharias, A. Rosch, M. Garst, Critical elasticity at zero and finite temperature. *Eur. Phys. J. Spec. Top.* **224**, 1021–1040 (2015).
37. D. N. Nichols, R. J. Sladek, H. R. Harrison, Elastic constants of V_2O_3 between 300 and 640 K: Anomalies near the high-temperature electrical transition. *Phys. Rev. B* **24**, 3025–3030 (1981).
38. S. Papanikolaou, R. M. Fernandes, E. Fradkin, P. W. Phillips, J. Schmalian, R. Sknepnek, Universality of liquid-gas Mott transitions at finite temperatures. *Phys. Rev. Lett.* **100**, 026408 (2008).
39. T. Furukawa, K. Miyagawa, H. Taniguchi, R. Kato, K. Kanoda, Quantum criticality of Mott transition in organic materials. *Nat. Phys.* **11**, 221–224 (2015).
40. V. Dobrosavljevic, *"Wigner-Mott quantum criticality: From 2D-MIT to ^{3}He and Mott organics", Contribution to: "Strong Correlation Phenomena around 2D Conductor-Insulator Transitions"*, S. V. Kravchenko, Ed. (Pan Stanford Publishing, 2016).
41. B. Hartmann, D. Zielke, J. Polzin, T. Sasaki, J. Müller, Critical slowing down of the charge carrier dynamics at the Mott metal-insulator transition. *Phys. Rev. Lett.* **114**, 216403 (2015).
42. Y. Kurosaki, Y. Shimizu, K. Miyagawa, K. Kanoda, G. Saito, Mott transition from a spin liquid to a Fermi liquid in the spin-frustrated organic conductor κ-$(ET)_2Cu_2(CN)_3$. *Phys. Rev. Lett.* **95**, 177001 (2005).
43. Y. Shimizu, H. Akimoto, H. Tsujii, A. Tajima, R. Kato, Mott transition in a valence-bond solid insulator with a triangular lattice. *Phys. Rev. Lett.* **99**, 256403 (2007).

44. I. Leonov, V. I. Anisimov, D. Vollhardt, Metal-insulator transition and lattice instability of paramagnetic V_2O_3. *Phys. Rev. B* **91**, 195115 (2015).
45. A. Jayaraman, D. B. McWhan, J. P. Remeika, P. D. Dernier, Critical behavior of the Mott transition in Cr-doped V_2O_3. *Phys. Rev. B* **2**, 3751–3756 (1970).
46. S. Populoh, P. Auban-Senzier, P. Wzietek, C. R. Pasquier, The power factor of Cr-doped V_2O_3 near the Mott transition. *Appl. Phys. Lett.* **99**, 171902 (2011).
47. A. G. Gavriliuk, I. A. Trojan, V. V. Struzhkin, Insulator-metal transition in highly compressed NiO. *Phys. Rev. Lett.* **109**, 086402 (2012).
48. S. Wang, J. Zhu, Y. Zhang, X. Yu, J. Zhang, W. Wang, L. Bai, J. Qian, L. Yin, N. S. Sullivan, C. Jin, D. He, J. Xu, Y. Zhao, Unusual Mott transition in multiferroic $PbCrO_3$. *Proc. Natl. Acad. Sci. U.S.A.* **112**, 15320–15325 (2015).
49. S. Liu, B. Phillabaum, E. W. Carlson, K. A. Dahmen, N. S. Vidhyadhiraja, M. M. Qazilbash, D. N. Basov, Random field driven spatial complexity at the Mott transition in VO_2. *Phys. Rev. Lett.* **116**, 036401 (2016).
50. R. Küchler, T. Bauer, M. Brando, F. Steglich, A compact and miniaturized high resolution capacitance dilatometer for measuring thermal expansion and magnetostriction. *Rev. Sci. Instrum.* **83**, 095102 (2012).
51. R. Pott, R. Schefzyk, Apparatus for measuring the thermal expansion of solids between 1.5 and 380K. *J. Phys. E Sci. Instrum.* **16**, 444–449 (1983).
52. H. Anzai, J. M. Delrieu, S. Takasaki, S. Nakatsuji, J.-i. Yamada, Crystal growth of organic charge-transfer complexes by electrocrystallization with controlled applied current. *J. Cryst. Growth* **154**, 145–150 (1995).
53. B. Hartmann, J. Müller, T. Sasaki, Mott metal-insulator transition induced by utilizing a glasslike structural ordering in low-dimensional molecular conductors. *Phys. Rev. B* **90**, 195150 (2014).
54. T. Hiramatsu, Y. Yoshida, G. Saito, A. Otsuka, H. Yamochi, M. Maesato, Y. Shimizu, H. Ito, H. Kishida, Quantum spin liquid: Design of a quantum spin liquid next to a superconducting state based on a dimer-type ET Mott insulator. *J. Mater. Chem. C* **3**, 1378–1388 (2015).
55. J. Müller, M. Lang, F. Steglich, J. A. Schlueter, A. M. Kini, T. Sasaki, Evidence for structural and electronic instabilities at intermediate temperatures in κ-$(BEDT\text{-}TTF)_2X$ for X=$Cu[N(CN)_2]Cl$, $Cu[N(CN)_2]Br$ and $Cu(NCS)_2$: Implications for the phase diagram of these quasi-two-dimensional organic superconductors. *Phys. Rev. B* **65**, 144521 (2002).
56. Y. Watanabe, H. Sato, T. Sasaki, N. Toyota, Lattice parameters of κ-$(BEDT\text{-}TTF)_2Cu[N(CN)_2]Br$. *J. Phys. Soc. Jpn.* **60**, 3608–3611 (1991).
57. M. de Souza, A. Brühl, Ch. Strack, B. Wolf, D. Schweitzer, M. Lang, Anomalous lattice response at the Mott transition in a quasi-2D organic conductor. *Phys. Rev. Lett.* **99**, 037003 (2007).

Acknowledgments: We acknowledge useful discussions with J. Schmalian, P. Kopietz, I. Paul, M. Zacharias, and S. Winter. **Funding:** The research was supported by the German Science Foundation via the Transregional Collaborative Research Center SFB/TR49 "Condensed Matter Systems with Variable Many-Body Interactions" and the Collaborative Research Center SFB 1143 "Correlated Magnetism: From Frustration to Topology." Work in Sendai was partly supported by the Japan Society for the Promotion of Science KAKENHI grant #JP25287080. Work at Argonne, in a U.S. Department of Energy Office of Science laboratory, is operated under contract #DE-AC02-06CH11357. J.A.S. acknowledges support from the Independent Research and Development program while serving at the NSF. **Author contributions:** M.L. conceived and supervised the project. Measurements of the relative length changes were performed by E.G. with contributions from R.S.M., U.T., B.W., and M.L. Theoretical description of the data was developed by M.G. with contributions from L.B. M.G. and E.G. analyzed the data. H.S., T.S., and J.A.S. grew the high-quality single crystals. M.L. wrote the paper with contributions from E.G. and M.G. All authors discussed the results and commented on the manuscript. **Competing interests:** The authors declare that they have no competing interests. **Data and materials availability:** All data needed to evaluate the conclusions in the paper are present in the paper and/or the Supplementary Materials. Additional data related to this paper may be requested from the authors.

Submitted 18 July 2016
Accepted 3 November 2016
Published 7 December 2016
10.1126/sciadv.1601646

Citation: E. Gati, M. Garst, R. S. Manna, U. Tutsch, B. Wolf, L. Bartosch, H. Schubert, T. Sasaki, J. A. Schlueter, M. Lang, Breakdown of Hooke's law of elasticity at the Mott critical endpoint in an organic conductor. *Sci. Adv.* **2**, e1601646 (2016).

Breakdown of Hooke's law of elasticity at the Mott critical endpoint in an organic conductor

Elena Gati, Markus Garst, Rudra S. Manna, Ulrich Tutsch, Bernd Wolf, Lorenz Bartosch, Harald Schubert, Takahiko Sasaki, John A. Schlueter and Michael Lang

Sci Adv **2** (12), e1601646.
DOI: 10.1126/sciadv.1601646